Influence of step-bunching on grazing incidence diffuse x-ray scattering

1999 J. Phys.: Condens. Matter 11 2661

(http://iopscience.iop.org/0953-8984/11/13/003)

J. Phys.: Condens. Matter **11** (1999) 2661–2668. Printed in the UK PII: S0953-8984(99)99109-9

Influence of step-bunching on grazing incidence diffuse x-ray scattering

J Clarke†, I Pape†, B K Tanner† and M Wormington‡

† Department of Physics, University of Durham, South Road, Durham DH1 3LE, UK
‡ Bede Scientific Inc., 14 Inverness Drive East, Suite G-104, Englewood, CO 80112, USA

Received 10 November 1998

Abstract. An asymmetry in the grazing incidence diffuse x-ray scatter from a 420 Å silver film grown on an offcut (111) silicon substrate has been interpreted as arising from fractal-like step-bunching of terraces at the substrate–layer interface. The variation of diffuse scatter with the component of scattering vector normal to the film surface indicates the presence of different lateral correlation lengths for the two interfaces.

1. Introduction

It has been well documented in recent years that under specific growth conditions Si(111), misorientated towards certain crystallographic orientations, will undergo the process of step-bunching [1]. This growth process is well understood and highly controllable, having very important applications in, for example, the enhancement of the giant magnetoresistance (GMR) effect in spin-valve devices [2, 3]. Independently a number of reports have documented the presence of asymmetries in grazing incidence diffuse x-ray scattering experiments where the asymmetries have been attributed to the presence of terraced structures on the surface of the samples [4–6]. In our previous studies of Co/Cu superlattices grown by molecular beam epitaxy (MBE) on $CuSi_3$ buffered (001) Si substrates, we observed a sharp peak in the diffuse scatter whilst rocking the sample at a fixed scattering vector [7]. This peak was offset from the specular scatter and this offset was seen to vary upon rotation of the sample about its surface normal. Since these diffuse scatter data can be fitted extremely well to a model of the interfaces based on the fractal model proposed by Sinha *et al* [8], we have suggested that it originates from non-uniformly bunched steps on the surface of the sample [9].

In this present paper we describe similar but more detailed observations made on a single layer of silver grown on an offcut Si(111) substrate under deposition conditions comparable with those known to induce step-bunching [2, 3]. Since this is a relatively simple system to study it has allowed us to confirm our original identification of the origin of the asymmetry in the diffuse scatter whilst also confirming the fact that under the correct growth conditions offcut Si(111) does indeed undergo step-bunching.

2. Experimental technique

Grazing incidence x-ray scattering measurements have been made on a single 420 Å silver layer, grown on an offcut Si(111) substrate at York University. The Si substrate, offcut by

0953-8984/99/132661+08$19.50

0.1° from the (111) orientation, was initially heated under UHV until the 7×7 reconstruction could be observed by *in situ* RHEED. During deposition of the silver film by molecular beam epitaxy (MBE), the Si substrate was held at a temperature of 150 °C.

The x-ray measurements were made using the two-circle diffractometer on station 2.3 at Daresbury SRS. A wavelength of 1.54 Å was selected, delivering, in this conventional reflectivity set-up, a count rate of 1×10^8 c.p.s. at the sample in a beam 100 μm high, 4 mm wide and with 30 arcseconds divergence.

Three types of x-ray measurement were undertaken. Specular ($\theta/2\theta$) scans recorded the intensity as the detector was swept at twice the angular rate of the sample, i.e. $\Phi = 2\theta$. This produced a scan parallel to the q_z axis in reciprocal space effectively mapping out the momentum transfer perpendicular to the sample surface. Longitudinal diffuse measurements were also made by scanning in a coupled $\theta/2\theta$ ratio but with the sample initially offset by $-0.1°$ from the specular condition. In reciprocal space these scans correspond to radial lines propagating away from the (000) point where they record the diffuse scatter present just below the specular ridge. By performing such scans we are then able to remove the forward diffuse scatter component from the specular allowing us to model the *true* specular scatter. Finally, transverse diffuse scans were performed by fixing the detector angle and scanning the sample. This corresponds to an arc nearly parallel to the q_x direction in reciprocal space effectively measuring the momentum transfer parallel to the samples surface. In real space these scans allow us to probe the diffuse scatter at either side of the specular ridge. The scattering geometries for such scans in real and reciprocal space are shown in figures 1 and 2 respectively.

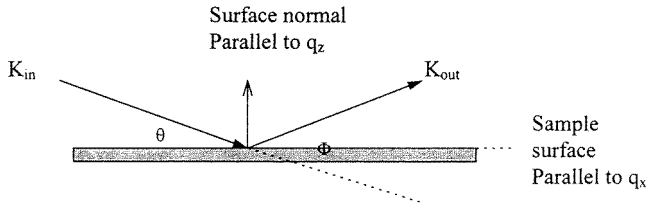

Figure 1. Real space scattering geometry for typical grazing incidence x-ray scattering experiment where θ is the angle of incidence and Φ the scattering angle.

3. Analytical method

The data were matched to simulations performed using the Bede GIXS code, which is based on a model of the interfaces treated within the distorted wave Born approximation (DWBA) of x-ray scattering as described by Sinha *et al* [8]. This model assumes a self-affine fractal interface with a cut-off determined by a correlation length ξ. While it represents a particular class of interface, it can be varied from gently undulating to very jagged depending on the fractal Hirst parameter h. Mathematically, this is incorporated through the isotropic auto-covariance function $C(r)$, between points in the interface separated by a distance r, given by

$$C(r) = \sigma^2 \exp[-(r/\xi)^{2h}] \tag{1}$$

where σ is the r.m.s. roughness. Where more than one interface exists, the effect of conformality between the roughness of successive interfaces i and j is modelled by generalizing this to

$$C_{ij}(r) = (\sigma_{ui}\sigma_{uj}\delta_{ij} + \sigma_{ci}\sigma_{cj}) \exp[-(r/\xi)^{2h}]. \tag{2}$$

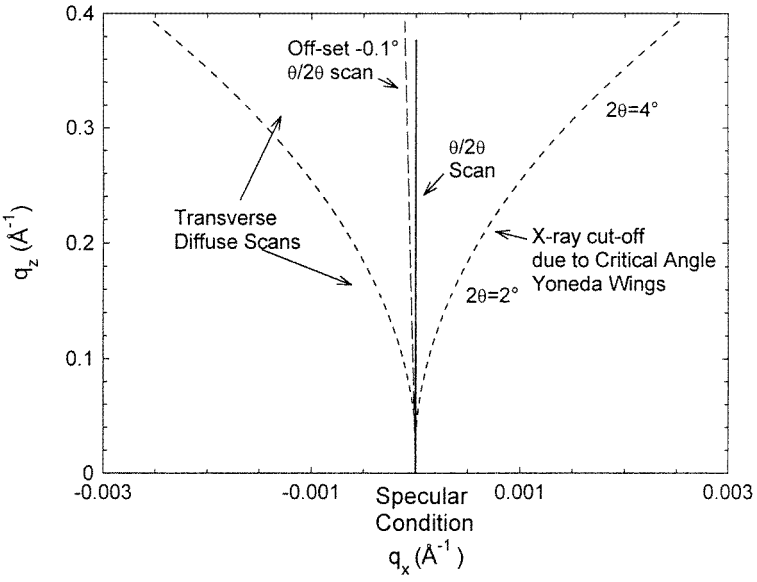

Figure 2. Reciprocal space scattering geometry, calculated for Si at $\lambda = 1.3926$ Å.

Here σ_c is the roughness which replicates perfectly the morphology of the interface from layer to layer and σ_u is the roughness which does not replicate at all. The total roughness σ_i at interface i is given by adding in quadrature the correlated and uncorrelated roughness, that is,

$$\sigma_i^2 = \sigma_{ci}^2 + \sigma_{ui}^2. \tag{3}$$

This model scales linearly with the number of layers and also permits an integral in the scattering cross section to be expanded into a standard form which may be tabulated. The result is a very rapid implementation of the calculation of the scattered intensity. The theory has been extended to incorporate the effects of compositional grading by inclusion of an error function electron density profile at the interface [10] and it has been shown that the compositional grading and true roughness can be separated through measurement of both specular and diffuse scattering.

For the present study, the code has been modified phenomenologically to include treatment of terraced interfaces. The electric fields in the sample are calculated using the mean interface position whereas the wavevectors, and corresponding scattering vectors, are calculated relative to the terrace. This results in the position of the diffuse scattering peak moving with respect to the specular scattering peak in the transverse diffuse scans, there being no shift in the position of the Yoneda wings.

4. Results

Shown in figure 3 is the specular and off-specular scatter recorded from the specimen. Simulations of the specular data, corrected for its diffuse background, were performed and the resulting best fit is shown as the solid line in the figure. Excellent agreement is seen between the critical angle (corresponding to the silver layer), the interference fringe period and amplitude and the overall fall-off of intensity as a function of scattering angle. The parameters required for the best fit are shown in figure 4. Transverse diffuse scans were performed for a range of scattering vectors and azimuthal angles. Shown in figure 5 is the diffuse scatter recorded from

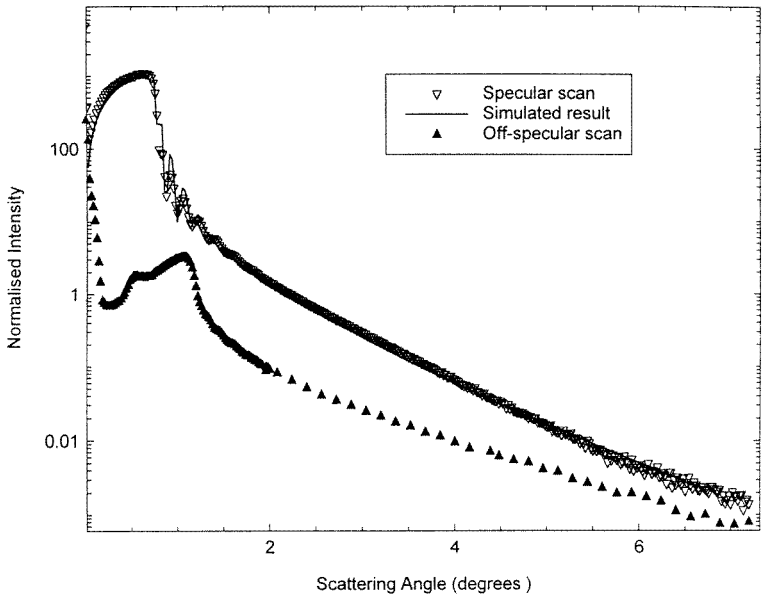

Figure 3. Specular and off-specular θ–2θ scans from the silver film. The solid line is a simulation of the measured true specular scatter from which the forward diffuse scatter, determined by the off-specular scan, has been subtracted.

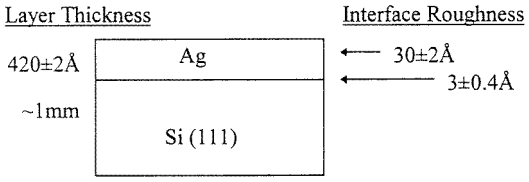

Figure 4. Best-fit parameters to the true specular scatter.

the sample for azimuthal angles of 0 and 180° at a fixed scattering vector. It is immediately apparent from these data that there exists a single broad peak in the diffuse scatter which is off-set from the sharp specular peak, the latter not changing its position on rotation about the azimuth. We see from figure 6 that the peak in the diffuse scatter precesses sinusoidally around the specular peak, exhibiting a maximum offset of $0.13 \pm 0.02°$. In addition, it is noted that the positions of the Yoneda wings at each end of the scan remain constant and that the specular peak lies midway between them.

The variation of diffuse intensity with scattering vector is illustrated in figure 7. This contains a series of transverse diffuse scans taken at several detector positions (scattering angle, 2θ) for a fixed azimuthal angle. From these data it is observed that as the scattering vector is increased the peak in the diffuse scatter becomes increasingly prominent.

Simulations of this diffuse scatter have been carried out using the Bede GIXS code which allows the inclusion of different correlation lengths in the model and also allows a terrace angle to be specified for the substrate (namely the angle between the average plane of the interface and the mean surface of the terraced regions). Figure 8 shows simulated transverse diffuse scans, obtained using this code, taken at identical scattering angles to the experimental data

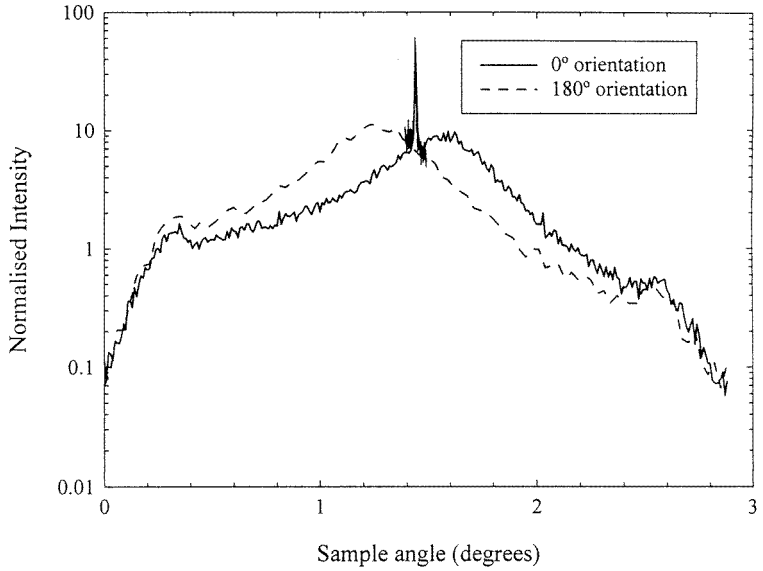

Figure 5. Transverse diffuse scans at different azimuthal angles.

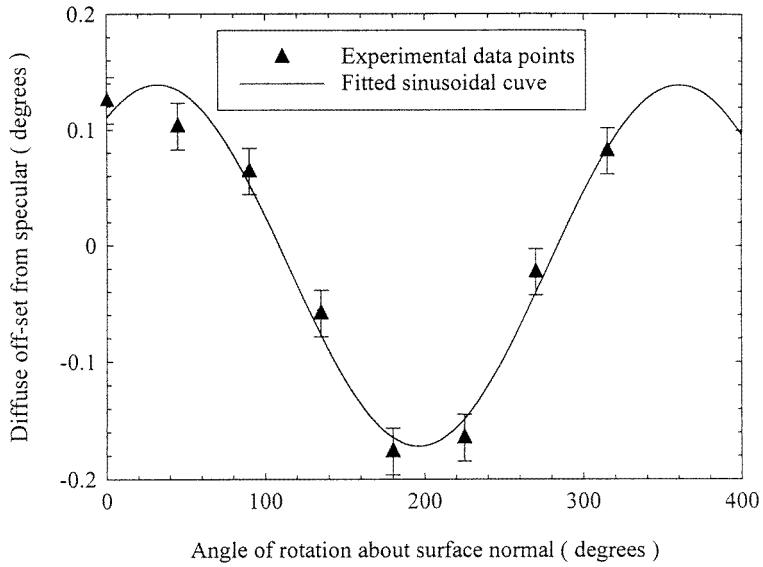

Figure 6. Angular separation of the specular and diffuse peaks as a function of azimuthal angle of rotation.

in figure 7. These simulations were obtained using the parameters shown in figure 4 with top and bottom surface correlation lengths of 1000 and 3000 Å respectively. In addition a terrace angle of 0.139° was specified in order to match accurately the position of the offset diffuse peak. Figure 9 shows the resulting best fit obtained with this model at a scattering vector of 1.281°.

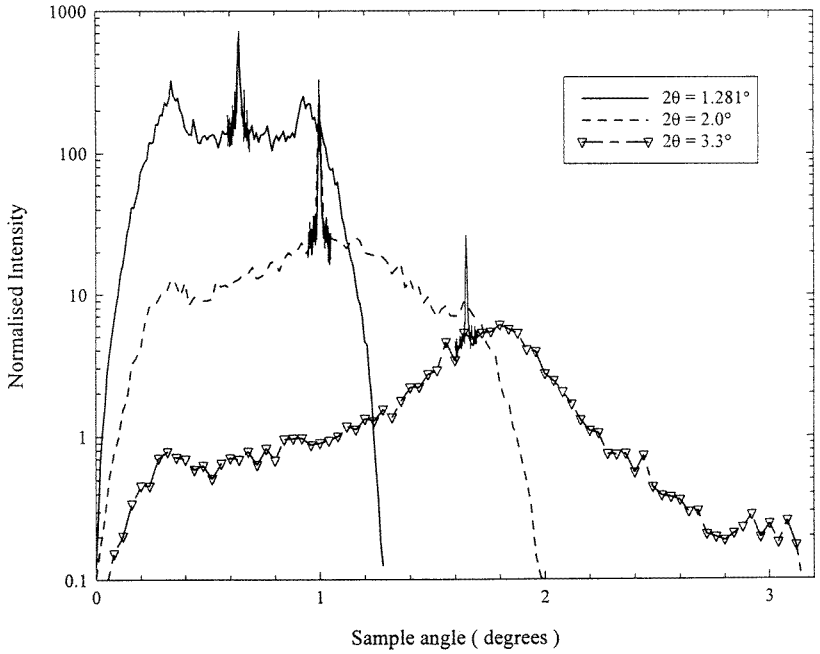

Figure 7. Transverse diffuse scans for different scattering angles showing the change in shape of the diffuse scatter, with loss of the central peak at low scattering angles.

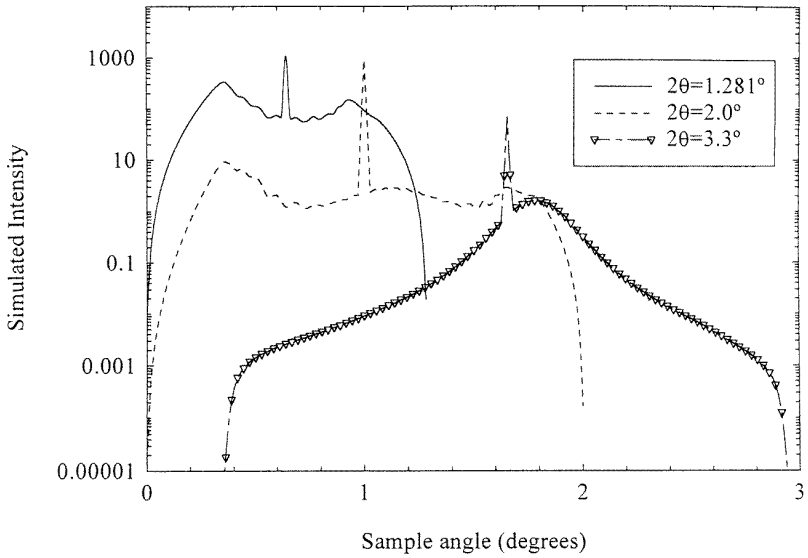

Figure 8. Simulated transverse diffuse scans obtained at the scattering angles shown in figure 7 demonstrating the same change in shape as was observed in the experimental data.

We were unable to determine the degree of conformality of the roughness between the lower interface and the top surface. Simulation of the off-specular diffuse scatter shows that for the large difference in roughness present here ($\sigma = 3$ and 30 Å for lower and upper surfaces

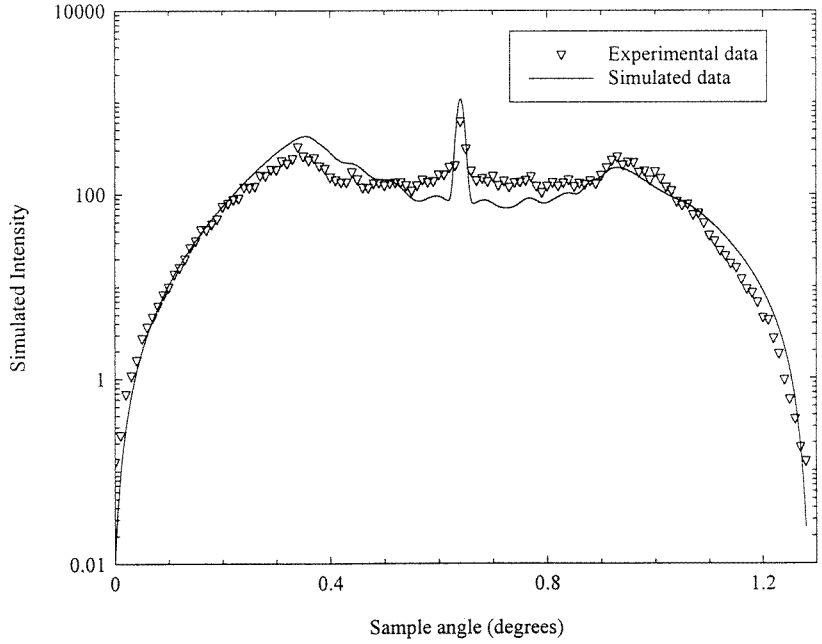

Figure 9. Best-fit simulation of a transverse diffuse scan taken at a scattering angle $2\theta = 1.281^\circ$.

respectively) identical, very weak Kiessig fringes occur in the off-specular scatter for both highly correlated and uncorrelated roughness.

5. Discussion

The presence of asymmetries in the diffuse scatter has been observed previously by several groups [4–6]. In all cases it has been ascribed to a preferential orientation of roughness at the interfaces and, by implication, terracing within the layers. As the specular scatter arises from the average plane of these terraced regions the effect of terracing is to introduce an offset between the diffuse and specular components. In the previous studies, the diffuse scatter was concentrated into two symmetric peaks either side of the specular ridge. These are characteristic of lateral periodicities on interfaces within the sample, which give rise to this diffraction grating effect. In the case of the silver sample however, only a single peak was observed, implying that no regular periodicities exist on its interfaces. Furthermore whereas previous studies found that the diffuse scatter exhibited a marked difference in shape along the q_x and q_y axes, the shape of the diffuse scatter from the silver sample was invariant as a function of azimuthal angle and just shifted in position. The constancy of the shape of this scatter implies a isotropic distribution of roughness length scales on the interfaces. This behaviour is very similar to that observed previously on the series of Co/Cu multilayers grown by MBE on Si(111) using a Cu_3Si buffer [7, 9].

It would appear that the above observations can be best described by an interface which has undergone step-bunching. In this case the diffuse scatter arises from local, isotropically rough, bunched regions separated by long terraces and which are at an angle to the average interface. These bunched regions can have the fractal character implicit in the model with which they have been simulated.

The resulting diffuse scatter is thus offset with respect to the specular peak and on rotation of the sample about its surface normal, this diffuse peak precesses sinusoidally about the specular position whilst remaining unchanged in shape. It is modelled by the GIXS code for a terraced interface, where we note that the specular peak and the Yoneda wings remain fixed as the azimuthal angle is varied [9], while the diffuse peak moves sinusoidally.

From our observation that the peak in the diffuse scatter only occurs at the higher scattering vectors, it can be implied that the terracing is confined to the lower interface. Hence, it is probable that the step-bunching was induced on the offcut silicon surface during processing. The growth conditions used in the wafer fabrication were consistent with this occurring [2, 3].

We note in both figures 7 and 8 that the peak in the diffuse scatter is not observed for small scattering angles. This suggests that the correlation length of the top surface is significantly shorter than that of the substrate–film interface and this conclusion is supported by the detailed simulations of the diffuse scatter and consistent with the proposed model of a terraced substrate surface.

6. Conclusions

We have shown that the asymmetry with respect to the specular scatter of the grazing incidence diffuse scatter from a thin silver film grown on a silicon substrate offcut by 0.1° from the (111) orientation can be explained as arising from fractal, non-uniformly bunched steps on the terraced interface between substrate and film. These measurements on a single film confirm the interpretation of the diffuse scatter from Co/Cu multilayers also grown on (111) oriented silicon [9] and help to explain why the fractal model is so successful in describing the diffuse scatter from MBE-grown films. There appear to be differing lateral correlation lengths on the two interfaces and this may be associated with lack of conformality between the substrate and air surfaces of the film. Due to the large difference in roughness of the two interfaces, we are unable to verify this last suggestion from the diffuse x-ray scatter.

Acknowledgment

Financial support from the Engineering and Physical Science Research Council is acknowledged.

References

[1] Bartlet N C, Williams E D, Phaneuf R J, Yang Y and Das Sarma S 1989 *J. Vac. Sci. Technol.* A **7** 1898
[2] Encinas A, Nguyen Van Dau F, Sussiau M, Schuhl A and Galtier P 1997 *Appl. Phys. Lett.* **71** 3299
[3] Nguyen Van Dau F, Sussiau M, Schuhl A and Galtier P 1997 *J. Appl. Phys.* **81** 4482
[4] Phang Y H, Teichert C, Lagally M G, Peticolos L J, Bean J C and Kasper E 1994 *Phys. Rev.* B **50** 14 435
[5] Sinha S K, Sanyal M K, Satija S K, Majkrzak C F, Neumann D A, Homma H, Szpala S, Gibaud A and Morkoc H 1994 *Physica* B **198** 72
[6] Neumann D A, Zabel H and Morkoc H 1983 *Appl. Phys. Lett.* **43** 59
[7] Pape I, Hase T P A, Tanner B K, Laidler H, Emmerson C, Shen T and Hickey B J 1996 *J. Magn. Magn. Mater.* **156** 373
[8] Sinha S K, Sirota E B, Garoff S and Stanley H B 1988 *Phys. Rev.* B **38** 2297
[9] Pape I, Hase T P A, Tanner B K and Wormington M 1998 *Physica* B **253** 278
[10] Wormington M, Pape I, Hase T P A, Tanner B K and Bowen D K 1996 *Phil. Mag. Lett.* **74** 211